 https://doi.org/10.3311/PPme.20360

Periodica Polytechnica Mechanical Engineering, 67(1), pp. 44–50, 2023

Energy Dissipation and Chemical Yield of an Ultrasound Driven Single Bubble

Csanád Kalmár[1*], Ferenc Hegedűs[1]

[1] Department of Hydrodynamic Systems, Faculty of Mechanical Engineering, Budapest University of Technology and Economics, Műegyetem rkp. 3., H-1111 Budapest, Hungary
[*] Corresponding author, e-mail: cskalmar@hds.bme.hu

Received: 21 April 2022, Accepted: 09 November 2022, Published online: 16 January 2023

Abstract

A detailed parameter study is made of chemically active spherical bubbles. The calculations apply an up-to-date chemical mechanism for pure oxygen initial content, taking into account pressure dependency, duplication of chemical reactions, and proper third-body efficiency coefficients. The chemical yield is defined as the amount of substance at the maximum bubble radius, and the dissipated power is approached in a relatively new method. The parameter study focuses on finding the parameter combinations where maximum yield and maximum energy efficiency arise for various chemical species (O_3, OH radical, H_2 and H_2O_2). Results show that the locations of maximum yield and efficiency points differ significantly, depending on the chemical species. Usually, neither chemical yield nor efficiency values arise at maximum pressure amplitude and minimum driving frequency (as one would presumably expect).

Keywords

acoustic cavitation, chemical yield, energy efficiency, sonochemistry

1 Introduction

Irradiating a liquid domain with high intensity and high-frequency ultrasound, micron-sized bubbles are formed [1, 2] in so-called bubble clusters [3, 4]. When the pressure amplitude extends Blake's critical threshold [5], the bubbles tend to grow even ten times the equilibrium size in the negative pressure phase. This is followed by a rapid compression in the positive pressure phase due to the high inertia of the liquid [6, 7]. The final temperature of the compression can reach several thousands of Kelvins, which induces chemical reactions inside the bubbles [8, 9]. This procedure is called sonochemistry, and it has been a heavily researched area in the last decades [10, 11].

One of the biggest challenges in sonochemical modelling is the validation of chemical mechanisms. Many authors work with several different models for different chemical compositions [12–14], and the results often alter significantly. Recently, we published a comprehensive study [15] about chemical modelling in sonochemistry, and we even suggested a state-of-the-art mechanism for a pure oxygen bubble.

Most of the papers focus on the maximizing chemical yield of various species [13, 16] in terms of bubble temperature, bubble size, or driving parameters. However, from a practical applications point of view, the energetic aspects cannot be avoided at some point; the amount of input power has to be taken into account in order to operate in optimal conditions. An obvious approach would be considering the acoustic power irradiated by the ultrasound transducer, which could be easily calculated from the driving parameters (pressure amplitude and frequency). However, this often leads to highly misleading conclusions due to a common phenomenon in sonochemical reactors called *acoustic shielding* [17]. This means that the acoustic radiation cannot penetrate the bulk liquid because the outer layers of the cluster absorb a significant amount of energy of the ultrasound. Consequently, the emitted acoustic power is not a good metric for the input power.

In our approach, we define input power as the dissipated power of a single bubble, which was introduced lately by several authors [18–20]. This avoids the possible miscalculations caused by the aforementioned shielding effect and gives a theoretical maximum efficiency that can be achieved by proper reactor operation.

In the present paper, a detailed, numerical parameter study is made, using a state-of-the-art chemical mechanism for purely oxygen bubble content. The chemical yield

Cite this article as: Kalmár, C., Hegedűs, F. "Energy Dissipation and Chemical Yield of an Ultrasound Driven Single Bubble", Periodica Polytechnica Mechanical Engineering, 67(1), pp. 44–50, 2023. https://doi.org/10.3311/PPme.20360

and energy efficiency are defined appropriately for applicational purposes. Yield and efficiency maps are constructed in order to explore optimal parameter combinations.

2 Chemical mechanism and the mathematical model

The chemical mechanism applied in this work was chosen based on the aforementioned comparison in our previous paper [15]. It was shown that it is crucial to use the best chemical mechanism available in order to draw quantitatively correct conclusions. The chemical model applied in our paper was developed in [21], and it was proven to be the best mechanism regarding bubbles saturated with pure oxygen. The model works with precisely validated Arrhenius-constants, and takes into account third body efficiencies, pressure-dependent and duplicated reactions as well. Here, only a brief introduction of the mathematical model is presented; the details of the full mechanism and the model parameters are described thoroughly in [15].

The rate of a chemical reaction is calculated by the modified Arrhenius equation as:

$$k = AT^b e^{-\frac{E}{\Re T}}, \tag{1}$$

where k is the (forward) reaction rate constant, T is temperature, $\Re$ is the universal gas constant, and A, b and E are the three Arrhenius-constants. This reaction rate is possibly modified by specific third-body efficiencies, pressure-dependent terms, or reaction duplication. The backward reaction rate is calculated by fulfilling proper thermodynamic conditions.

The production rate of each chemical species is determined by:

$$\dot{\omega}_k = \sum_{i=1}^{I} \nu_{ki} q_i, \quad (k = 1...K), \tag{2}$$

where ν_{ki} are the stochiometric coefficients in reaction i, q_i is the net reaction rate of reaction i, and K is the total number of chemical species.

As for physical conditions, the bubble is considered as spherically symmetric and isolated. The gas content is treated as ideal gas, the pressure, temperature, and concentration of the species are spatially uniform. Heat fluxes are modeled with a proper boundary layer approximation [22], and evaporation of water is estimated with the approach of [23] assuming non-equilibrium phase change. The different thermodynamic properties (specific heat, enthalpy, entropy) are calculated via NASA polynomials. Again, the interested reader is referred to [15] for details.

The radial dynamics of the isolated bubble is described by the Keller-Miksis equation in the form of:

$$\begin{aligned}&\left(1-\frac{\dot{R}}{c_L}\right)R\ddot{R}+\left(1-\frac{\dot{R}}{3c_L}\right)\frac{3}{2}\dot{R}^2\\&=\left(1+\frac{\dot{R}}{c_L}+\frac{R}{c_L}\frac{d}{dt}\right)\frac{p_L-p_\infty}{\rho_L},\end{aligned} \tag{3}$$

where $R(t)$ is the unknown function of bubble radius, c_L is the sound speed in liquid, ρ_L is the liquid density, p_L is the pressure at the bubble wall and p_∞ is the far field pressure, excited by ultrasound as $p_\infty = P_\infty + p_A \sin 2\pi ft$. Here, P_∞ is the ambient pressure, p_A and f are the ultrasound amplitude and frequency, respectively. As a boundary condition, the internal pressure is expressed as $p = p_L + 2\sigma / R + 4\mu_L \dot{R} / R$, where σ and μ_L are the surface tension and the dynamic viscosity of the liquid, respectively.

The energy balance between the bubble interior and the bulk liquid is characterized by the first law of thermodynamics in the form of:

$$\overline{c}_v \dot{T} = -p\dot{V} + \dot{Q}, \tag{4}$$

where $\overline{c}_v$ is the average molar heat capacity of the mixture at constant volume, V is the volume of the bubble and $\dot{Q}$ is the sum of reaction heats and heat fluxes.

The amount of dissipated power of a single bubble is calculated by the approach of Jamshidi and Brenner [19]. Accordingly, the dissipated power is categorized into three main sources: thermal, viscous and radiation dissipation, namely:

$$\Pi_{th} = \frac{1}{T_p}\int_0^{T_p} -\left(p\left(1+\frac{\dot{R}}{c_L}\right)\frac{R}{c_L}\dot{p}\right)\dot{V}dt, \tag{5}$$

$$\Pi_v = \frac{1}{T_p}\int_0^{T_p} 16\pi\mu_L\left(R\dot{R}^2+\frac{R^2\dot{R}\ddot{R}}{c_L}\right)dt, \tag{6}$$

$$\Pi_r = \frac{4\pi}{T_p c_L}\int_0^{T_p} R^2\dot{R}\left(\dot{R}p+R\dot{p}-\frac{1}{2}\rho_L\dot{R}^3-\rho_L R\dot{R}\ddot{R}\right)dt, \tag{7}$$

where $T_p = 1/f$ is the period of the excitation, Π_{th}, Π_v and Π_r are the thermal, viscous and radiation dissipation in Watt units, respectively. The total dissipated power is the sum of the three components written as $\Pi_w = \Pi_{th} + \Pi_v + \Pi_r$. It should be noted that the dissipation is averaged over one acoustic cycle. This amount of power will be regarded as input power when the energy efficiencies are calculated.

3 Equation system and numerical method

The set of ordinary differential equations consists as follows. The Keller-Miksis equation (Eq. (3)) is of second order, which could be rewritten into two first-order ones. The internal temperature is obtained from the first law of thermodynamics (Eq. (4)). The temporal evolution of the concentration of each chemical species is determined as:

$$\dot{c}_k = \dot{\omega}_k - c_k \frac{\dot{V}}{V}, \tag{8}$$

with the amount of water vapor being adjusted by the net evaporation rate.

The value of Π_w is being integrated during the numerical simulation, as well. These altogether conclude in a system of ordinary differential equations of size $3 + K + 1 = K + 4$. In our case, ten different chemical species are considered, meaning the size of the equation system is 14.

The system is solved numerically with the 4th or 5th order Runge-Kutta-Cash-Karp scheme, with embedded error estimation. Both absolute and relative tolerances were set to 10^{-10}. The initial conditions were set to the equilibrium state ($R_0 = R_E$, $T_0 = T_\infty$), and the initial concentrations were set as vapor content being saturated (meaning $p_{0,H_2O} = p_v^*$) and the remaining content were initiated to be purely oxygen.

The numerical simulations were performed on a GPU hardware with an in-house written ODE solver package [24, 25], developed specifically to maintain detailed parameter studies. The investigated control parameters were the pressure amplitude p_A and driving frequency f, with the ranges shown in Table 1. The third parameter – the equilibrium radius – was set to 2 μm. Other fixed parameters are indicated in Table 2.

4 Results and discussion

4.1 Definition of chemical yield

Solving the equation system at a certain parameter combination, one can obtain the time curves of bubble radius $R(t)$, internal temperature $T(t)$ and concentrations for each species $c_k(t)$. Fig. 1 shows the times curves at $f = 50$ kHz and $p_A = 1.8$ bar. Notice, that the concentrations are converted to amount of substance in moles, the bubble radius is nondimensionalized with R_E, and the time axes are also

Table 1 Ranges of control parameters

Parameter name	Abbrev.	Range	Resolution
Pressure amplitude	p_A	1–2 bar	512 (linear)
Driving frequency	f	20–1000 kHz	512 (logarithmic)

Table 2 Values of fix parameters

Parameter name	Abbrev.	Value
Liquid sound speed	c_L	1483 m/s
Liquid density	ρ_L	998.2 kg/m^3
Surface tension	σ	$71.97 \cdot 10^{-3}$ N/m
Dynamic viscosity	μ_L	0.001 Pa s
Ambient pressure	P_∞	1 bar
Ambient temperature	T_∞	300 K
Universal gas constant	$\Re$	8.31446 J / mol K
Acc. coeff. for evap.	α_M	0.35
Saturated vapor pressure	p_v^*	2338.1 Pa
Equilibrium radius	R_E	2 μm

in nondimensional form of $\tau = t \cdot f$. This means $\tau = 1$ corresponds to one full acoustic cycle. Observe that only the convergent part of the solution is plotted and τ is shifted to be 0 at the start.

It is apparent from Fig. 1 that the bubble expands drastically in the negative pressure phase. After, it collapses rapidly due to the high inertia of the liquid. At the end of the collapse, the temperature peaks at around 6000 K, where most of the water vapor content dissociates, and other species appear. After the rapid compression, the temperature

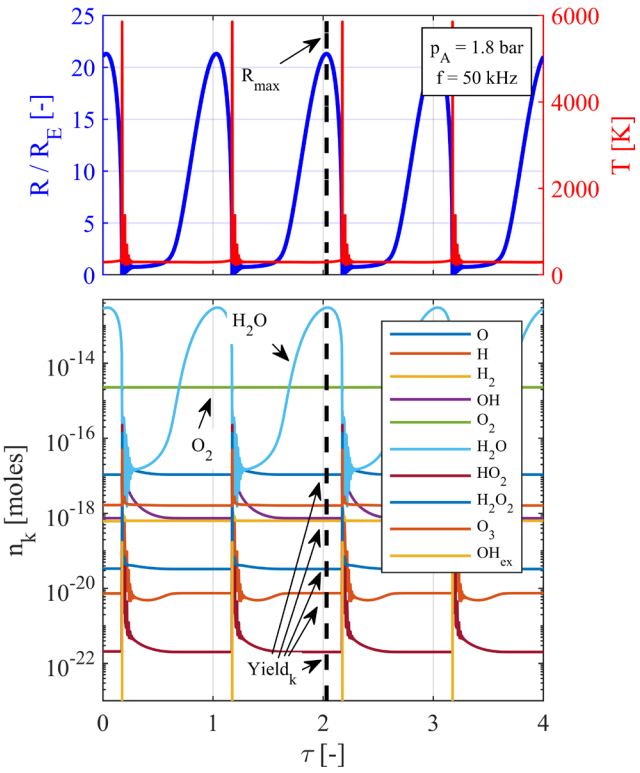

Fig. 1 Time curves of bubble radius (blue) and temperature (red) on the top chart, amount of substance in moles of each species in the bottom chart. $f = 50$ kHz and $p_A = 1.8$ bar. The chemical yields are at the intersection with the dashed line.

resets to around the ambient value, and the amount of species mostly stagnate. This dynamical equilibrium repeats itself during the oscillation.

For further investigation and parameter study, the *chemical yield* is defined as the amount of substance at the maximum bubble radius. On Fig. 1, these values are indicated by the intersections with the vertical dashed line. It can be observed that different yields belong to each chemical species. The main reason for this definition is that for further applications, this amount of substance will be available *after* switching off the acoustic radiation.

During the evaluation, only the chemical yield and the dissipated power will be investigated further, obtained from a specific parameter combination.

4.2 Mapping the chemical yields

Performing the parameter scan according to Table 1, one can create chemical yield maps as a function of driving frequency and pressure amplitude. Fig. 2 shows the maps for H_2, O_3, OH radical and H_2O_2. Note, that the frequency and yield values are on logarithmic scales, and the maximum yield values are marked with red dots on the maps. The charts show that the chemical yield for each species starts to grow at $p_A \approx 1.2$ bar at $f = 20$ kHz, but this *threshold* shifts toward higher amplitudes with increasing frequency. Above $f \approx 500$ kHz, there is no significant chemical activity, except maybe for OH radical.

Species H_2, O_3 and H_2O_2 all share a very interesting property: the highest yield values settle in a well-bounded band, starting from around $p_A = 1.2$–1.6 bar at $f = 20$ kHz, and as frequency increases, the corresponding pressure amplitude increases, too. The band is the narrowest for H_2O_2, and the widest for O_3. However, the maximum yield values emerge exactly at $f = 20$ kHz in the case of H_2, but for O_3 and H_2O_2, the maximum values happen to be at the other side of the "bands" (see the marked maximum values with red points). This is quite counterintuitive behavior, as one would expect increasing yield with increasing pressure amplitude at first glance, as the collapses get stronger with pressure amplitude.

To demonstrate the existence of this optimal pressure amplitude (at fixed driving frequency), the time curves are plotted in Fig. 3 at $p_A = 1.73$ (dotted lines) and 1.5 (continuous lines) bar. Note that in the bottom chart, only the amount of H_2 is shown for better understandability. Also, the time axes are shifted so that the strong collapse is at $\tau = 0$. Although at the strong collapse, both the temperature and molecule number peak at higher values for $p_A = 1.73$ bar, after the first afterbounce, the molecule number decreases

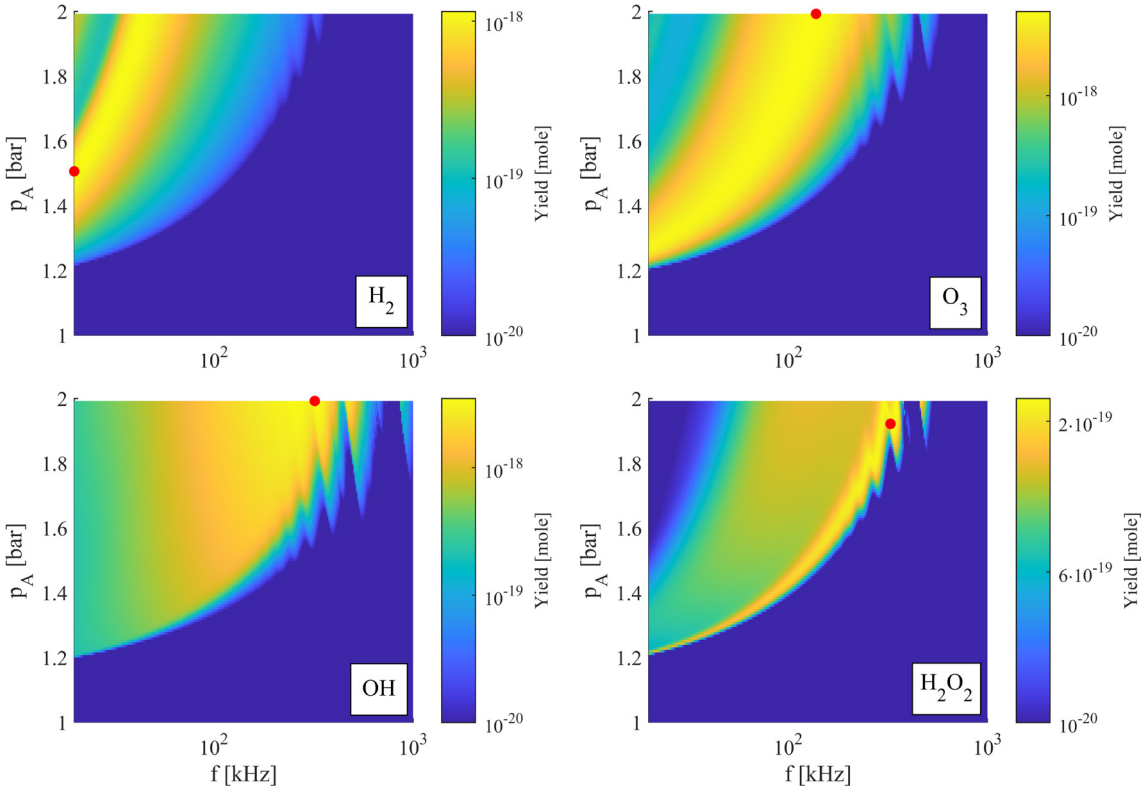

Fig. 2 Chemical yield maps of H_2, O_3, OH and H_2O_2 as a function of driving frequency and pressure amplitude. The frequency and yield scales are logarithmic. The maximum yield values for each species are marked with red dots.

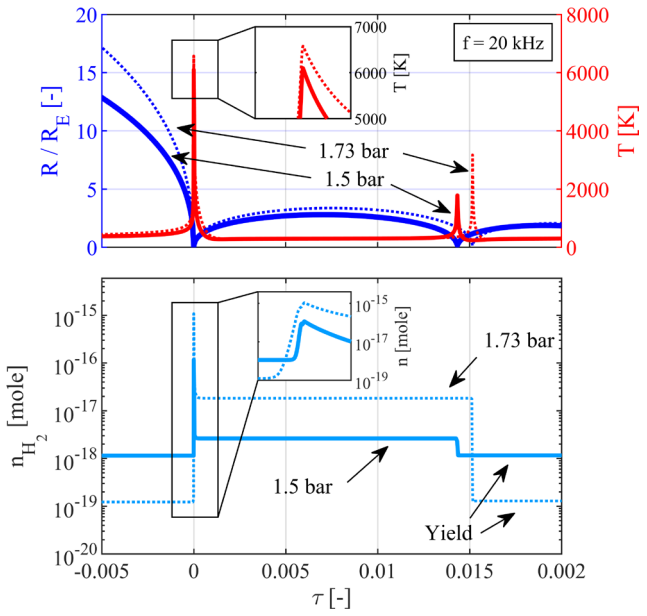

Fig. 3 Comparison of the time curves at p_A = 1.73 bar (dotted lines) and 1.5 bar (continuous lines). The driving frequency is 20 kHz. Only the amount of H_2 is shown at the bottom chart.

to a lower value than that of p_A = 1.5 bar. This is the reason for the overall chemical yield being higher for the lower pressure amplitude. This effect is most probably the result of the numerous complex chemical reactions occurring simultaneously, and a simple explanation might not even exist.

The existence of optimal frequency range was previously demonstrated experimentally by several authors [26–28] for H_2O_2 yield. They showed that higher chemical production occurred at f = 355 kHz than at 20 kHz. This is in really good qualitative agreement with our numerical results, see the maximum yield of H_2O_2 in the bottom right chart of Fig. 2.

OH radical does not show this kind of trend; its yield grows rather monotonically with driving frequency until the sonochemical threshold.

4.3 Energy efficiency inquiries

In most sonochemical applications, high chemical yield is necessary, however, in long-term operation, high energy efficiency is required, as well. Here, we define *efficiency* as the ratio of chemical yield and input power, defined in Section 2. by Eqs. (5)–(7). This means that different efficiency values belong to each chemical species. In this manner, all parameter combinations can be represented with one efficiency value for each chemical component. Note that the efficiencies are in mole/Watt units.

Fig. 4 shows the efficiency maps as a function of pressure amplitude and driving frequency, for the same 4 species as in Fig. 2. The frequency and efficiency values are on logarithmic scales again, and the maximum values are also marked with red dots, as well. The maps for the 4 species

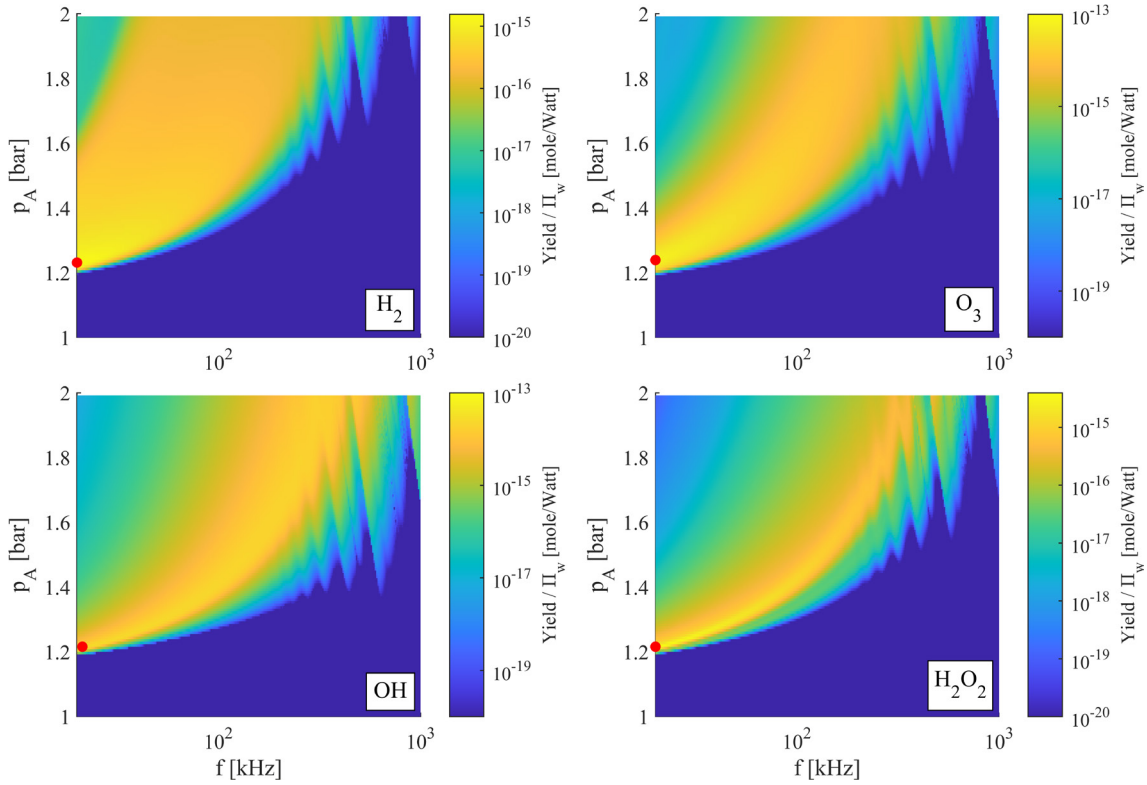

Fig. 4 Efficiency maps of H_2, O_3, OH and H_2O_2 as a function of driving frequency and pressure amplitude. The frequency and yield scales are logarithmic. The maximum efficiency values for each species are marked with red dots.

are rather similar: the efficiency grows drastically around p_A = 1.2 bar at f = 20 kHz, and the bands that appeared in Fig. 2 are absent here, too, even for the OH radical. This is probably the consequence of two main reasons. First, the chemical yield also has similar band-like property, except for the OH radical. Second, the dissipated (input) power grows drastically as pressure amplitude increases.

Another interesting point is that the maximum efficiencies arise at the lowest frequency (20 kHz) for all 4 species, right above the sonochemical threshold, around p_A = 1.2 bar. Observe, that these points alter immensely from the maximum yields, especially for O_3, OH and H_2O_2. This implies that the optimal operating strategy heavily depends on which chemical species do we need, and whether we want to maximize the chemical yield or the efficiency. This consequence strongly suggests highly sophisticated chemical modeling in sonochemistry in order to obtain the desired operation.

5 Summary

In the present study, a state-of-the-art chemical mechanism is applied for a chemically active spherical bubble saturated with oxygen. The model includes proper third-body efficiencies, pressure-dependence, and reaction duplication, as well. The system of ODEs was solved numerically on GPUs with an in-house made program package.

A detailed parameter study was made on the pressure amplitude – driving frequency plane. The investigation focused on the chemical yield and energy efficiency of specific chemical components.

The results show that the chemical yield distribution alters heavily depending on the species considered. The highest chemical yield values settle in a well-defined band; this was examined via time curves of H_2. It was also shown that the pressure amplitude and driving frequency corresponding to the maximum yield differs remarkably depending on chemical species considered.

The efficiency of the sonochemical reactor was defined with the aid of dissipated power. It was shown that maximum efficiency arises at the lowest driving frequency, just above the sonochemical threshold in pressure amplitude.

As a consequence, we can state that comprehensive knowledge about the yield and efficiency maps are essential for an optimal reactor operation.

Acknowledgement

The research reported in this paper is part of project no. BME-NVA-02, implemented with the support provided by the Ministry of Innovation and Technology of Hungary from the National Research, Development and Innovation Fund, financed under the TKP2021 funding scheme. The research was also supported by the New National Excellence Program of the Ministry of Human Capacities (project no. ÚNKP-21-5-BME-369).

The authors would also like to acknowledge the kind help of Tamás Turányi, István Gy. Zsély and Máté Papp from the Chemical Kinetics Laboratory, Institute of Chemistry of Eötvös Loránd University, Budapest, Hungary.

References

[1] Klapcsik, K. "GPU accelerated numerical investigation of the spherical stability of an acoustic cavitation bubble excited by dual-frequency", Ultrasonics Sonochemistry, 77, 105684, 2021. https://doi.org/10.1016/j.ultsonch.2021.105684

[2] Tuziuti, T., Yasui, K., Iida, Y. "Spatial study on a multibubble system for sonochemistry by laser-light scattering", 12(1–2), pp. 73–77, 2005. https://doi.org/10.1016/j.ultsonch.2004.05.010

[3] Rosselló, J. M., Lauterborn, W., Koch, M., Wilken, T., Kurz, T., Mettin, R. "Acoustically induced bubble jets", Physics of Fluids, 30(12), 122004, 2018. https://doi.org/10.1063/1.5063011

[4] Haghi, H., Sojahrood, A. J., Kolios, M. C. "Collective nonlinear behavior of interacting polydisperse microbubble clusters", Ultrasonics Sonochemistry, 58, 104708, 2019. https://doi.org/10.1016/j.ultsonch.2019.104708

[5] Blake, F. G. "The onset of cavitation in liquids", In: Technical Memorandum, Acoustics Research Laboratory, Harvard University, Cambridge, MA, USA, 1949, 12.

[6] Sojahrood, A. J., Earl, R., Haghi, H., Li, Q., Porter, T. M., Kolios, M. C., Karshafian, R. "Nonlinear dynamics of acoustic bubbles excited by their pressure-dependent subharmonic resonance frequency: influence of the pressure amplitude, frequency, encapsulation and multiple bubble interactions on oversaturation and enhancement of the subharmonic signal", Nonlinear Dynamics, 103(1), pp. 429–466, 2021. https://doi.org/10.1007/s11071-020-06163-8

[7] Klapcsik, K. "Dataset of exponential growth rate values corresponding non-spherical bubble oscillations under dual-frequency acoustic irradiation", Data in Brief, 40, 107810, 2022. https://doi.org/10.1016/j.dib.2022.107810

[8] Yasui, K., Tuziuti, T., Kozuka, T., Towata, A., Iida, Y. "Relationship between the bubble temperature and main oxidant created inside an air bubble under ultrasound", The Journal of Chemical Physics, 127(15), 154502, 2007. https://doi.org/10.1063/1.2790420

[9] Kalmár, C., Klapcsik, K., Hegedűs, F. "Relationship between the radial dynamics and the chemical production of a harmonically driven spherical bubble", Ultrasonics Sonochemistry, 64, 104989, 2020. https://doi.org/10.1016/j.ultsonch.2020.104989

[10] Stricker, L., Lohse, D. "Radical production inside an acoustically driven microbubble", Ultrasonics Sonochemistry, 21(1), pp. 336–345, 2014. https://doi.org/10.1016/j.ultsonch.2013.07.004

[11] Kerboua, K., Hamdaoui, O. "Influence of reaction heats on variation of radius, temperature, pressure and chemical species amounts within a single acoustic cavitation bubble", Ultrasonics Sonochemistry, 41, pp. 449–457, 2018. https://doi.org/10.1016/j.ultsonch.2017.10.001

[12] Yasui, K., Kato, K. "Bubble dynamics and sonoluminescence from helium or xenon in mercury and water", Physical Review E, 86(3), 036320, 2012. https://doi.org/10.1103/PhysRevE.86.036320

[13] Kerboua, K., Hamdaoui, O. "Numerical investigation of the effect of dual frequency sonication on stable bubble dynamics", Ultrasonics Sonochemistry, 49, pp. 325–332, 2018. https://doi.org/10.1016/j.ultsonch.2018.08.025

[14] Rashwan, S. S., Dincer, I., Mohany, A. "A unique study on the effect of dissolved gases and bubble temperatures on the ultrasonic hydrogen (sonohydrogen) production", International Journal of Hydrogen Energy, 45(41), pp. 20808–20819, 2020. https://doi.org/10.1016/j.ijhydene.2020.05.022

[15] Kalmár, C., Turányi, T., Zsély, I. G., Papp, M., Hegedűs, F. "The importance of chemical mechanisms in sonochemical modelling", Ultrasonics Sonochemistry, 83, 105925, 2022. https://doi.org/10.1016/j.ultsonch.2022.105925

[16] Yasui, K., Kato, K. "Numerical simulations of sonochemical production and oriented aggregation of $BaTiO_3$ nanocrystals", Ultrasonics Sonochemistry, 35, pp. 673–680, 2017. https://doi.org/10.1016/j.ultsonch.2016.05.009

[17] van Iersel, M. M., Benes, N. E., Keurentjes, J. T. F. "Importance of acoustic shielding in sonochemistry", Ultrasonics Sonochemistry, 15(4), pp. 294–300, 2008. https://doi.org/10.1016/j.ultsonch.2007.09.015

[18] Louisnard, O. "Nonlinear attenuation of sound waves by inertial cavitation bubbles", Physics Procedia, 3(1), pp. 735–742, 2010. https://doi.org/10.1016/j.phpro.2010.01.093

[19] Jamshidi, R., Brenner, G. "Dissipation of ultrasonic wave propagation in bubbly liquids considering the effect of compressibility to the first order of acoustical Mach number", Ultrasonics, 53(4), pp. 842–848, 2013. https://doi.org/10.1016/j.ultras.2012.12.004

[20] Sojahrood, A. J., Haghi, H., Karshafian, R., Kolios, M. C. "Nonlinear model of acoustical attenuation and speed of sound in a bubbly medium", In: 2015 IEEE International Ultrasonics Symposium (IUS), Taipei, Taiwan, 2015, pp. 1–4. ISBN 978-1-4799-8182-3 https://doi.org/10.1109/ULTSYM.2015.0086

[21] Varga, T., Olm, C., Nagy, T., Zsély, I. G., Valkó, É., Pálvölgyi, R., Curran, H. J., Turányi, T. "Development of a joint hydrogen and syngas combustion mechanism based on an optimization approach", International Journal of Chemical Kinetics, 48(8), pp. 407–422, 2016. https://doi.org/10.1002/kin.21006

[22] Toegel, R., Gompf, B., Pecha, R., Lohse, D. "Does water vapor prevent upscaling sonoluminescence?", Physical Review Letters, 85(15), 3165, 2000. https://doi.org/10.1103/PhysRevLett.85.3165

[23] Fujikawa, S., Akamatsu, T. "Effects of the non-equilibrium condensation of vapour on the pressure wave produced by the collapse of a bubble in a liquid", Journal of Fluid Mechanics, 97(3), pp. 481–512, 1980. https://doi.org/10.1017/S0022112080002662

[24] Hegedűs, F. "Massively Parallel GPU ODE Solver", [computer program] Available at: www.gpuode.com/downloads-docs--links.html [Accessed: 08 November 2022]

[25] Hegedűs, F. "Program package MPGOS: challenges and solutions during the integration of a large number of independent ODE systems using GPUs", Communications in Nonlinear Science and Numerical Simulation, 97, 105732, 2021. https://doi.org/10.1016/j.cnsns.2021.105732

[26] Kanthale, P., Ashokkumar, M., Grieser, F. "Sonoluminescence, sonochemistry (H_2O_2 yield) and bubble dynamics: Frequency and power effects", Ultrasonics Sonochemistry, 15(2), pp. 143–150, 2008. https://doi.org/10.1016/j.ultsonch.2007.03.003

[27] Brotchie, A., Ashokkumar, M., Grieser, F. "Sonochemistry and sonoluminescence under simultaneous high- and low-frequency irradiation", Journal of Physical Chemistry C, 112(22), pp. 8343–8348, 2008. https://doi.org/10.1021/jp8006987

[28] Brotchie, A., Grieser, F., Ashokkumar, M. "Sonochemistry and sonoluminescence under dual-frequency ultrasound irradiation in the presence of water-soluble solutes", The Journal of Physical Chemistry C, 112(27), pp. 10247–10250, 2008. https://doi.org/10.1021/jp801763v